

Article

Forward Current Transport Properties of AlGa_N/Ga_N Schottky Diodes Prepared by Atomic Layer Deposition

Hogyoung Kim ^{1,*} , Seok Choi ² and Byung Joon Choi ^{2,*}

¹ Department of Visual Optics, Seoul National University of Science and Technology (Seoultech), Seoul 01811, Korea

² Department of Materials Science and Engineering, Seoul National University of Science and Technology (Seoultech), Seoul 01811, Korea; yeshuaarmy@naver.com

* Correspondence: hogyoungkim@seoultech.ac.kr (H.K.); bjchoi@seoultech.ac.kr (B.J.C.); Tel.: +82-2-970-6233 (H.K.)

Received: 14 January 2020; Accepted: 21 February 2020; Published: 24 February 2020



Abstract: Atomic layer deposited AlGa_N on Ga_N substrate with different thicknesses was prepared and the electron transport mechanism of AlGa_N/Ga_N Schottky diodes was investigated. Above 348 K, both 5 and 10 nm thick AlGa_N showed that the thermionic emission model with inhomogeneous Schottky barrier could explain the forward current transport. Analysis using a dislocation-related tunneling model showed that the current values for 10 nm thick AlGa_N was matched well to the experimental data while those were not matched for 5 nm thick AlGa_N. The higher density of surface (and interface) states was found for 5 nm thick AlGa_N. In other words, a higher density of surface donors, as well as a thinner AlGa_N layer for 5 nm thick AlGa_N, enhanced the tunneling current.

Keywords: AlGa_N/Ga_N; dislocation-related tunneling; surface donors

1. Introduction

Among III-nitride materials, AlGa_N/Ga_N heterostructures have gained much interest due to the applications in high-temperature, high-voltage, and high-frequency electronic devices [1–3]. In particular, AlGa_N/Ga_N-based high electron mobility transistors (HEMTs) are commonly used because two-dimensional electron gas (2DEG) located just below the AlGa_N/Ga_N interface can be easily obtained with high conductivity. The electron sheet densities of 10^{13} cm⁻² were found to be obtained by using AlGa_N barriers when the Al content is typically 20–25% [3]. However, the large reverse leakage current occurring in AlGa_N/Ga_N HEMTs increase the noise at low-frequency and leads to current collapse, limiting the applicability of such devices [4]. Most of all, the leakage current flowing through the extended defects such as threading dislocations (TDs) are inevitably generated because of the large lattice mismatch and the different thermal expansion coefficients between (In,Al)Ga_N film and sapphire (or Si) substrate [5–7].

Several works have been performed to investigate the current transport mechanisms in AlGa_N-based devices. The barrier thinning which was caused by unintentional surface-defect donors was found to enhance the tunneling current, causing large leakage currents through (Al)Ga_N Schottky interfaces [8]. The reverse leakage current in AlGa_N/Ga_N was successfully analyzed in terms of a trap-assisted Poole–Frenkel (PF) emission [9]. Ha et al. suggested that the dominant current transport mechanism in AlGa_N/Ga_N Schottky diodes with CF₄ plasma treatment is the PF emission arising from fluorine-related deep traps into the continuum states related to dislocations [10]. It was found that the AlInN/Ga_N Schottky diode has a higher Schottky barrier but a larger reverse leakage current than an AlGa_N/Ga_N Schottky diode, which was attributed to higher defect density and higher tunneling current [11]. In atomic layer deposition (ALD), Al₂O₃, Al–Al and Al–O–H bonds have been

suppressed significantly by replacing the conventional H₂O source with O₃ and the density of positive bulk/interface charges was reduced to as low as $9 \times 10^{11} \text{ cm}^{-2}$ [12].

The ALD growth having a low-temperature and self-limiting growth mechanism can offer many advantages such as high uniformity, high conformality, and accurate thickness control [13], which can be applied to temperature-sensitive devices and flexible substrates like polymers. The Al_xGa_{1-x}N growth by ALD is utilized to modulate the bandgap from 6.2 eV (AlN) to 3.4 eV GaN, which is beneficial to design AlGaN-based devices. However, there is limited investigation into ALD-AlGaN and GaN [14,15], as compared to the intensive investigation of ALD-AlN. In this work, we grew AlGaN on GaN substrate by ALD and characterized the forward current transport properties in AlGaN/GaN Schottky contacts.

2. Materials and Methods

The ALD growth of AlGaN on *c*-plane (0001) GaN substrate was carried out using a thermal ALD system after native oxide removal process in an HCl:H₂O (1:1) solution. Both 5 and 10 nm thick AlGaN layers were grown at 335 °C using trimethylaluminum (TMA), triethylgallium (TEG), and NH₃ as Al, Ga, and N precursors, respectively. The ALD reaction was composed of TMA (TEG) feeding, N₂ purge, NH₃ feeding, and N₂ purge. AlGaN growth was done by the combination of GaN and AlN reactions with a pulse ratio of 1:1, corresponding to Al_{0.85}Ga_{0.15}N. According to the X-ray photoelectron spectroscopy (XPS) analysis, we found that the dominant peak in the Al 2*p* core-level spectra shifted to lower binding energy with the increase of AlN thickness due to a strong Al–Al peak, which was associated with the strain relaxation generated from the lattice mismatch between AlN and GaN [16]. In other words, when the thickness of AlN exceeded ~10 nm, the strain relaxation affected the overgrown AlN film quality. Figure 1a shows the XPS core-level spectrum obtained from 10 nm thick AlGaN surface, revealing no clear evidence of the Al–Al peak. This indicates that the effect of strain relaxation is insignificant. In order to minimize the effect of strain relaxation, we prepared relatively thin AlGaN layers such as 5 and 10 nm in this work. In order to characterize the electrical properties, AlGaN/GaN Schottky diodes were fabricated with a 50 nm thick Pt front contact (diameter: 500 μm) and a 100 nm thick Al contact was deposited over the entire back surface. Figure 1b shows the schematic layer structures of the devices. Current–voltage (*I*–*V*) and capacitance–voltage (*C*–*V*) measurements were carried out with a Keithley 238 current source and an HP 4284A LCR meter, respectively.

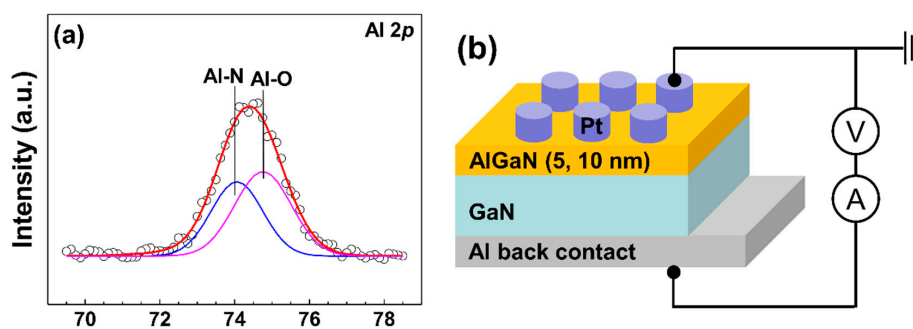


Figure 1. (a) X-ray photoelectron spectroscopy (XPS) Al 2*p* core-level spectrum obtained from 10 nm thick AlGaN surface and (b) schematic layer structures of the devices.

3. Results

Figure 2 shows the forward *I*–*V* data obtained at various temperatures. Using the thermionic emission (TE) model [17], the barrier heights were calculated. Here, we calculated the theoretical effective Richardson constant using the equation, $A^* = 2\pi q m^* k^2 / h^3$, where h is Planck's constant and m^* is the effective electron mass in AlGaN [18] and obtained the Richardson constant of Al_{0.85}Ga_{0.15}N as $40.0 \text{ A cm}^{-2} \text{ K}^{-2}$. The barrier height vs. temperature is described as $\Phi_B = \Phi_B - q\sigma_0^2 / 2kT$, where

$\bar{\Phi}_B$ is the zero-bias mean barrier height and σ_0 is the standard deviation. The plots of Φ_B vs. $1/2kT$ are shown in Figure 3a. The barrier heights for 10 nm thick AlGaN are higher than those for 5 nm thick AlGaN. The linear fits to plots of Φ_B vs. $1/2kT$ were applied to the temperature ranges of 325–425 K and 348–435 K, respectively, for 5 and 10 nm thick AlGaN. The linear fits yielded the values of $\bar{\Phi}_B = 1.55$ eV and $\sigma_0 = 0.19$ V for 5 nm thick AlGaN and the values of $\bar{\Phi}_B = 1.98$ eV and $\sigma_0 = 0.22$ V for 10 nm thick AlGaN. The modified Richardson plot with the lateral barrier inhomogeneity considered is described as follows:

$$\ln(I_0/T^2) - q^2\sigma_0^2/2k^2T^2 = \ln(AA^*) - \bar{\Phi}_B/kT \tag{1}$$

where I_0 is the reverse bias saturation current and A is the Schottky contact area. Figure 3b shows plots of $\ln(I_0/T^2) - q^2\sigma_0^2/2k^2T^2$ vs. $1/kT$. The intercepts at the ordinate produced modified Richardson constants of 44.8 and 44.4 $\text{Acm}^{-2}\text{K}^{-2}$, respectively, for 5 and 10 nm thick AlGaN. These values are similar to the theoretical value of 40.0 $\text{Acm}^{-2}\text{K}^{-2}$ for $\text{Al}_{0.85}\text{Ga}_{0.15}\text{N}$. Therefore, the forward current flows for AlGaN/GaN Schottky contacts can be explained by the TE model with Schottky barrier inhomogeneity.

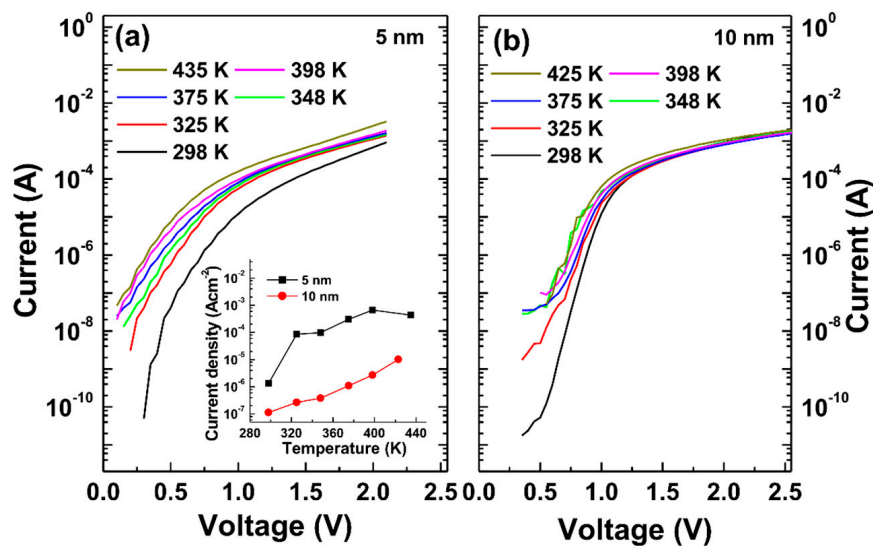


Figure 2. Current–voltage (I – V) data obtained at various temperatures: (a) 5 nm and (b) 10 nm thick AlGaN samples. The inset in (a) shows the reverse leakage current densities at -10 V.

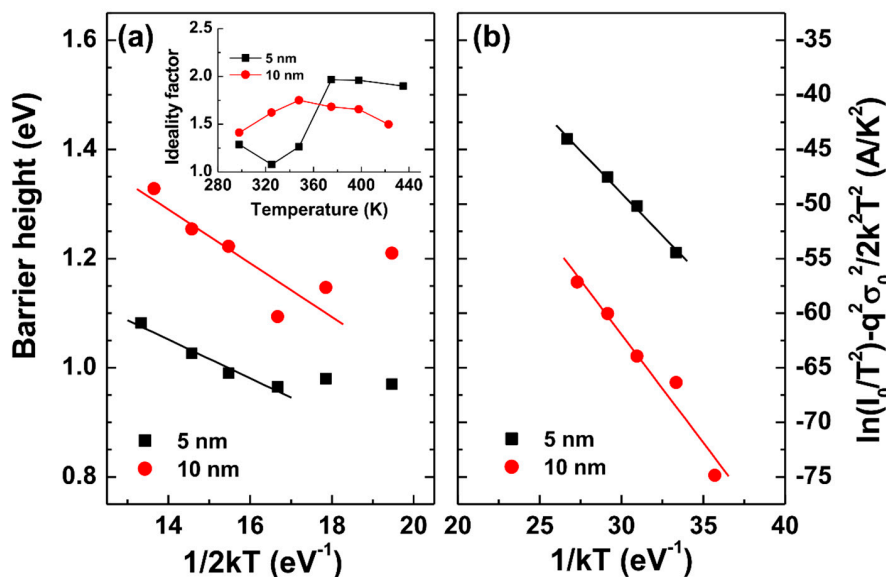


Figure 3. (a) Barrier height vs. $1/2kT$ plots and (b) modified Richardson plots. The inset in (a) shows the ideality factors.

To clarify the current transport mechanism more thoroughly, other transport components were considered comprehensively. The total current I_{TOT} , was assumed to be the combination of different transport mechanisms, given by [19]:

$$I_{TOT} = I_{TE} + I_{GR} + I_{TU} + I_{LE} \quad (2)$$

$$I_{TE} = I_{TE}^0 [\exp\{q(V - IR_S)/kT\} - 1] \quad (3)$$

$$I_{GR} = I_{GR}^0 [\exp\{q(V - IR_S)/2kT\} - 1] \quad (4)$$

$$I_{TU} = I_{TU}^0 [\exp\{q(V - IR_S)/E_0\} - 1] \quad (5)$$

$$I_{LE} = (V - IR_S)/R_{Sh} \quad (6)$$

where I_{TE} is the TE current, I_{GR} is the generation-recombination (GR) current, I_{TU} is the tunneling current (TU), and I_{LE} is the leakage current. $I_{TE}^0 = AA^*T^2 \exp(-\Phi_B/kT)$ (Φ_B : barrier height), I_{GR}^0 and I_{TU}^0 are the saturation currents of TE, GR, and TU components, respectively. $E_0 = E_{00} \coth(E_{00}/kT)$ is a parameter, where $E_{00} = q\hbar/2(N_d/m_e\epsilon_S)^{1/2}$ is the tunneling characteristic energy. R_S is the series resistance, which can be extracted from the curves where the I - V data begin to saturate and R_{Sh} is the shunt resistance. We fitted the experimental forward I - V curves to theoretical I - V data by taking I_{GR}^0 , I_{GR}^0 , I_{TU}^0 , and E_0 as fitting parameters. The experimental and fitted data at 298 K for 10 nm thick AlGaIn are shown in Figure 4 as an example.

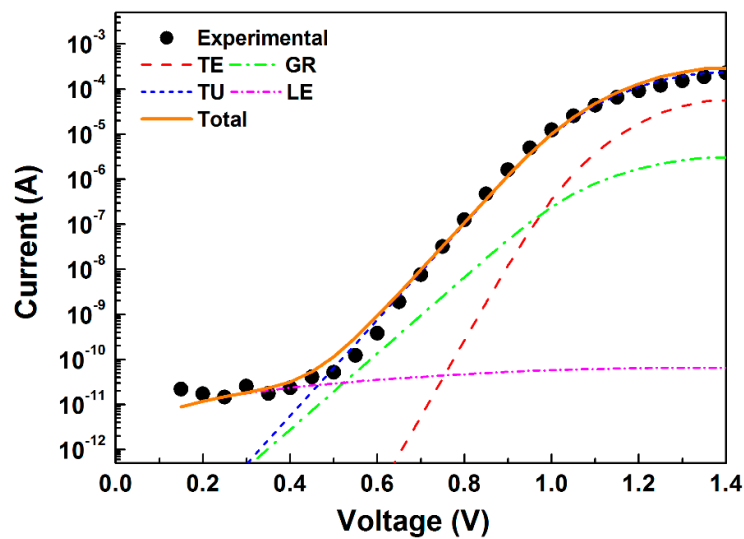


Figure 4. The fitting results of the forward I - V data at 298 K for a 10 nm thick AlGaIn sample are shown.

The barrier heights were calculated from I_{TE}^0 values of the TE component at different temperatures, which are shown in Figure 5a. The barrier heights showed very little temperature dependence for 5 nm thick AlGaIn, but these increased slightly with temperature for 10 nm thick AlGaIn. The relation between barrier height and bandgap energy (E_g) is roughly approximated as $\Phi_B \cong E_g/3$ [20]. The bandgap of $\text{Al}_{0.85}\text{Ga}_{0.15}\text{N}$ was found to be about 5.65 eV based on the argument by Pelá et al. [21]. Then, the barrier height can be obtained as 1.88 eV. This value is higher than the values in Figure 5a but is closer to the zero-bias mean barrier height of 1.98 eV for 10 nm thick AlGaIn. The flat-band barrier height was also determined using the barrier height and the ideality factor (n), which is given by [22]:

$$\Phi_{Bf} = n\Phi_B - (n - 1)kT/q \ln(N_C/N_D) \quad (7)$$

where N_C is the density of states at the conduction band and N_D is the carrier concentration. Under the flat-band condition, the electric field in the semiconductor is zero and the effects of image force

lowering and tunneling on the I - V properties are negligible. Figure 5b shows the obtained flat-band barrier heights. At higher temperatures (above 348 K), the values for both samples are closer to the value of 1.88 eV.

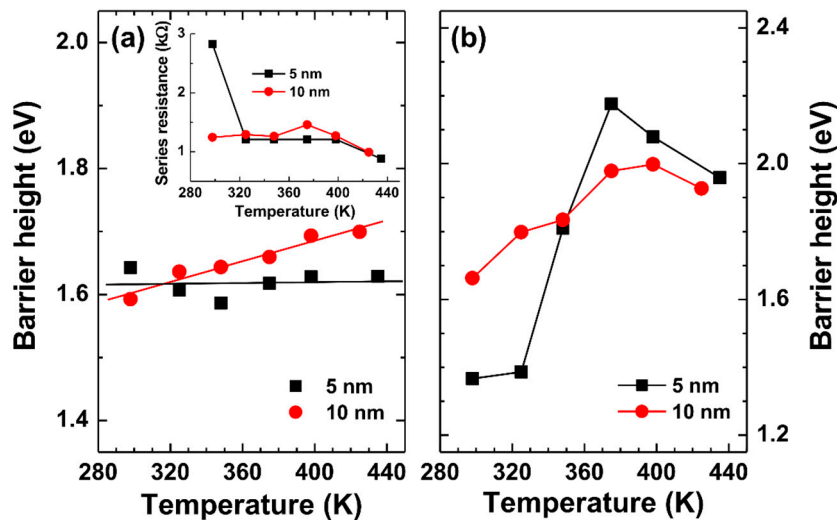


Figure 5. (a) Barrier heights obtained from thermionic emission (TE) component and (b) flat-band barrier heights. The inset in (a) shows the series resistances obtained from the fitting.

According to the dislocation-governed tunneling current model, the tunneling saturation current at 0 K can be described as [20]:

$$I_{TU}^0(0) = qAv_D N_{dis} \exp(-\Phi_B/E_t(0)) \quad (8)$$

where v_D ($\sim 1.5 \times 10^{13} \text{ s}^{-1}$ [23]) is the Debye frequency and N_{dis} is the dislocation density. Figure 6 shows the tunneling saturation current (I_{TU}^0) and the barrier energy (E_t). We extrapolated the linear fitting to the data in Figure 6 to attain I_{TU}^0 and E_t at 0 K. The barrier energy revealed a weak temperature dependence, indicating that the tunneling current is dominant. The tunneling saturation currents deviated from linearity at low temperatures and thus, some data were not included in the fitting. Finally, the dislocation densities were calculated to be 6.16×10^5 and $1.38 \times 10^{10} \text{ cm}^{-2}$, respectively, for 5 and 10 nm thick AlGaIn. Figure 7a shows the atomic force microscopy (AFM) surface image of 5 nm thick AlGaIn measured over $1 \mu\text{m} \times 1 \mu\text{m}$ scan area. The randomly distributed dark pits are observed over all the scan area. The small pits for GaN surface are known to represent the threading dislocations (TDs) with mixed and screw components where step edges meet, and pure edges meet when the components are on a terrace [24]. The values of TDs for $\text{Al}_{0.7}\text{Ga}_{0.3}\text{N}$ grown by metalorganic chemical vapor deposition (MOCVD) were also obtained from AFM images, which were found to be $2.5 \times 10^9 \text{ cm}^{-2}$. [25]. In this regard, we assumed that the density of pits are comparable to the density of TDs. The densities of these pits were measured to be $5.8 \times 10^{10} \text{ cm}^{-2}$ for 5 nm thick AlGaIn. As shown in Figure 7b the AFM image of 10 nm thick AlGaIn does not reveal clearly distributed dark pits (though dark regions are observed). Even though we tried to obtain AFM images from different regions, we could not get an image similar to that of the 5 nm thick AlGaIn. Nevertheless, it is possible to assume that the density of TDs would not decrease (or increase) significantly after increasing the AlGaIn thickness from 5 to 10 nm. Both 5 and 10 nm thick AlGaIn might have similar densities of TDs. Consequently, the density of TDs from AFM is similar to the value of $1.38 \times 10^{10} \text{ cm}^{-2}$ from 10 nm thick AlGaIn but is much higher than that from 5 nm thick AlGaIn. This implies that the dislocation-related tunneling current transport is the dominant mechanism in 10 nm thick AlGaIn. However, such a mechanism cannot be applied to 5 nm thick AlGaIn.

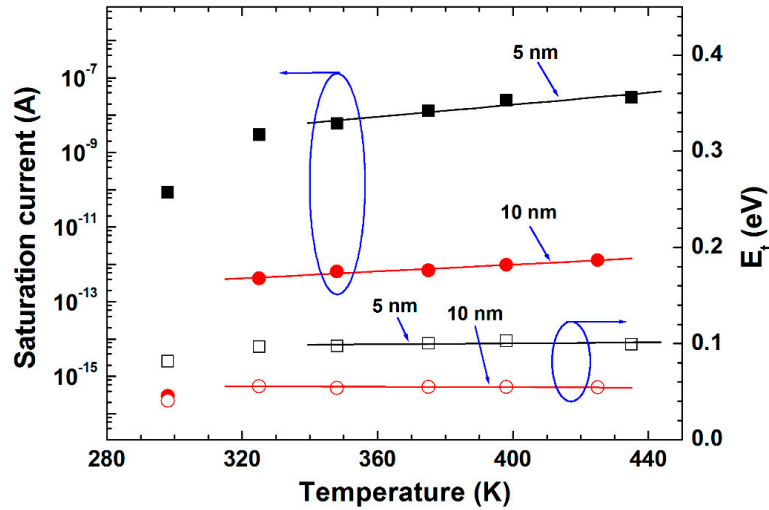


Figure 6. Tunneling saturation current and barrier energy vs. temperature.

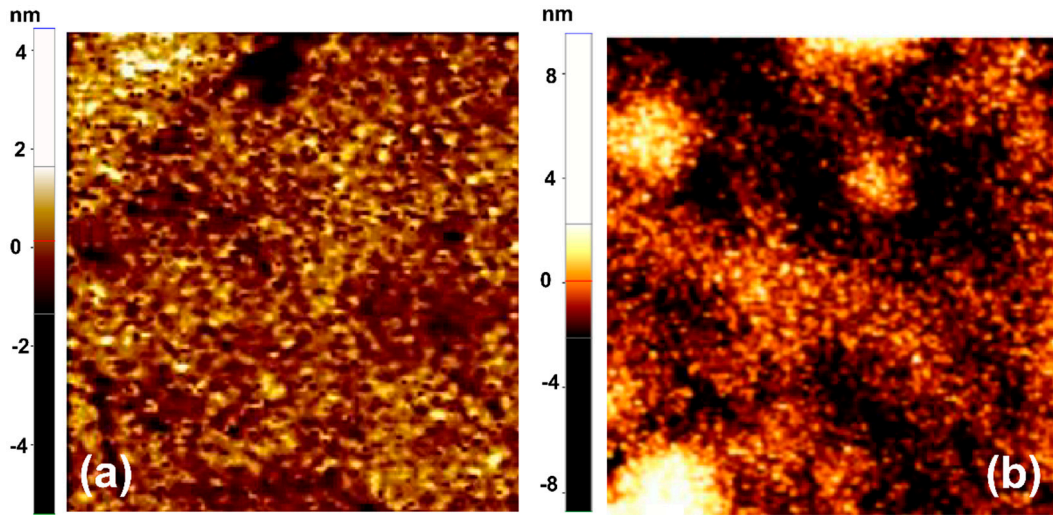


Figure 7. Atomic force microscope (AFM) images of (a) 5 nm and (b) 10 nm thick AlGaIn surface scanned over 1 $\mu\text{m} \times 1 \mu\text{m}$.

Figure 8a shows the $C-V$ data measured at room temperature. Here, $C-V$ characterization was performed at a frequency of 100 kHz to reduce the measurement error arising from the series resistance. The carrier concentration vs. depth was obtained, as shown in Figure 8b. The carrier concentration of $\sim 8 \times 10^{16} \text{ cm}^{-3}$ was obtained for 10 nm thick AlGaIn, similar to the value provided by the vendor. However, 5 nm thick AlGaIn was found to have a much higher value of $\sim 8 \times 10^{17} \text{ cm}^{-3}$. For n -type semiconductors, the Schottky barrier height is:

$$\Phi_B = qV_{bi} + kT/q \ln(N_C/N_d) = \Phi_m - \Phi_s + kT/q \ln(N_C/N_d) \tag{9}$$

with $\Phi_s = qV_0 + \chi + q|V_S|$, where $\Phi_m = 5.65 \text{ eV}$ is the work function of Pt [26], Φ_s is the surface work function of AlGaIn, χ is the electron affinity of AlGaIn, and qV_S is the surface band bending energy. By assuming that the electron affinity vs. x in $\text{Al}_x\text{Ga}_{1-x}\text{N}$ ($\chi_{\text{GaIn}} = 4.2 \text{ eV}$ and $\chi_{\text{AlIn}} = 2.05 \text{ eV}$) varies linearly [18], we obtained $\chi = 2.37 \text{ eV}$ for $\text{Al}_{0.85}\text{Ga}_{0.15}\text{N}$. Then, the barrier height can be written as:

$$\Phi_B = \Phi_m - \chi - q|V_S| = 3.28 - q|V_S| \tag{10}$$

By using the barrier heights from C - V measurements, the surface state density (N_S) was calculated through the following equation [27]:

$$q|V_S| = \frac{(qN_S)^2}{2\varepsilon\varepsilon_0N_D} \quad (11)$$

where ε is the dielectric constant of AlGaIn. The surface state densities at AlGaIn surface were found to be 3.9×10^{12} and $1.1 \times 10^{12} \text{ cm}^{-2}$, respectively, for 5 and 10 nm thick AlGaIn. This clearly indicates the higher surface state density for 5 nm thick AlGaIn. According to the thin surface barrier (TSB) model, the presence of surface donors can reduce the barrier width so that electrons tunnel through the thinner potential barrier easily [8,28]. Nitrogen vacancies and oxygen impurities in AlGaIn may be the origin of surface donors [29,30].

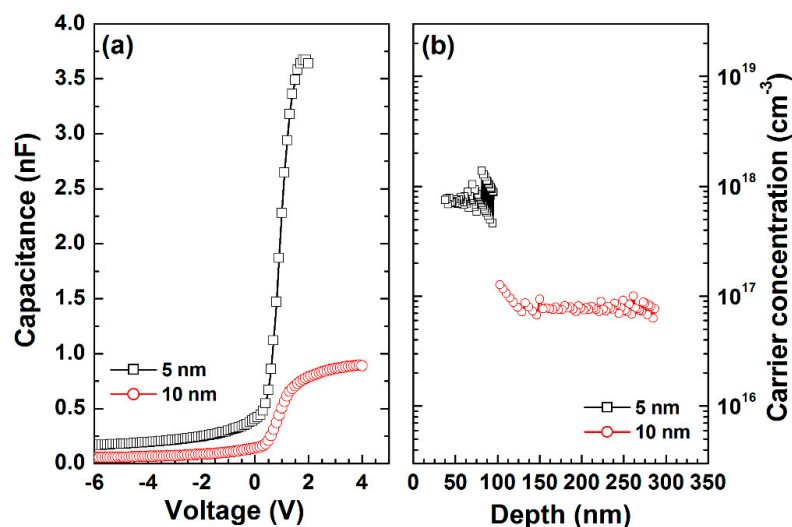


Figure 8. (a) Capacitance–voltage (C - V) characteristics measured at 100 kHz and (b) carrier concentration profiles vs. depth.

Because the interface states of a Schottky diode at the metal/semiconductor interface cannot follow the high-frequency signal, they do not contribute to the capacitance at high frequencies. Hence, the measured capacitance at a high-frequency consists of space-charge capacitance ($C \approx C_{SC}$). At low-frequencies, the total capacitance consists of the space-charge capacitance (C_{SC}) and the interface capacitance (C_{it}), which can be described as $C = C_{SC} + C_{it}$ [31]. The interface state density (N_{it}) can be written as [32]:

$$N_{it} = \frac{C_{it}}{qA} \quad (12)$$

The interface state energy (E_{it}) below the conduction band (E_C) at the semiconductor surface is given by $E_C - E_{it} = \Phi_B - qV$ [31,32]. The high and low-frequency C - V characteristics were obtained at 500 and 1 kHz, respectively. Using Equation (12), the interface state density was calculated over the depletion region. Here, we conjecture that both the energy states at the AlGaIn/GaN interface and near the AlGaIn surface might contribute to the interface state density. As shown in Figure 9, the interface state density for 5 nm thick AlGaIn was found to be higher. As a result, higher interface state density and a thinner AlGaIn barrier layer might enhance the tunneling current for 5 nm thick AlGaIn (i.e., direct tunneling could occur significantly) while the tunneling current is related to the TDs for 10 nm thick AlGaIn (i.e., trap assisted tunneling might occur through TDs). Figure 10 shows the schematic band structures for each sample describing the dominant current transport mechanism.

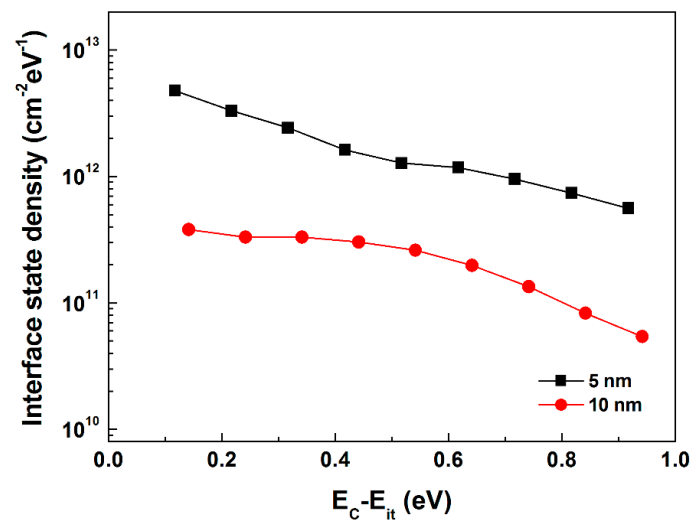


Figure 9. The energy distribution curves of the interface states obtained from the high- and low-frequency C - V characteristics.

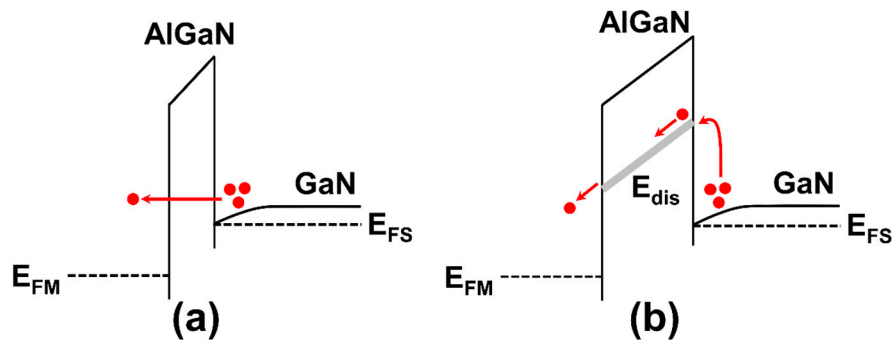


Figure 10. Schematic band diagrams presenting the dominant current transport under forward bias conditions for (a) 5 and (b) 10 nm thick AlGaIn.

As shown in Figure 8a, both samples show that the transition from depletion to accumulation occurred above 0 V, indicating that negative charges are present in the AlGaIn layer. Normally AlGaIn/GaN Schottky diodes and HEMTs have the transition voltages as negative values [11,33]. Systematic investigation of thermal annealing on AlGaIn/GaN HEMTs with different fluorine plasma treatment revealed the positive shift in the C - V characteristics with the increasing of the plasma power, which negatively shifted after thermal annealing [34]. It was explained by the fact that F^- ions introduced the acceptor-like states in the AlGaIn barrier layer and subsequent annealing eliminated some plasma-induced trap states. When acceptor-like defects are present, C - V curves stretch out in a positive direction [35]. Oxygen plasma treatment on AlGaIn/GaN HEMTs was found to cause a positive shift, reducing the content of the Al component in the AlGaIn barrier layer and depleting channel electrons [36]. The mechanism for positive flatband voltage shift and the depletion of electron gas due to oxygen plasma treatment was explained by gradual conversion of the AlGaIn barrier layer into an AlON/GaON structure [36]. The acceptor-like traps were associated with the oxidation of the recessed AlGaIn surface during ALD growth [12]. Analysis on the X-ray photoelectron spectroscopy for 10 nm thick AlGaIn (not shown) showed that the atomic percentage of oxygen atoms was about 15% in the AlGaIn layer, indicating that the AlGaIn layer is highly oxidized. Furthermore, 2DEG density according to the method by Lv et al. [37] was calculated to be about 1.1×10^{12} cm⁻² for both samples. This is too low compared to other works [37,38]. During the ALD growth, many acceptor-like defects might be formed in the AlGaIn layer and then, the electrons from the surface donors were captured while moving from the AlGaIn surface to the AlGaIn/GaN interface, lowering the 2DEG density and forming the negative charges. Based on the study using post metallization annealing, it was proposed

that the charges caused by interfacial defects could be passivated and neutralized through an H₂-based annealing [39]. Thus, thermal annealing on ALD-AlGa_N will be necessary to improve the interfacial quality of AlGa_N/Ga_N structure.

4. Conclusions

We characterized the current transport properties of AlGa_N/Ga_N Schottky diodes with an ALD-grown AlGa_N layer. At higher temperatures (above 348 K), both 5 and 10 nm thick AlGa_N showed that the TE model with Schottky barrier inhomogeneity was appropriate to explain the current flow. Higher barrier height for 10 nm thick AlGa_N was obtained compared to 5 nm thick AlGa_N. We fitted the experimental *I*–*V* data to the theoretical values with the consideration of various transport mechanisms. The dislocation-governed tunneling model was matched well to the experimental data for 10 nm thick AlGa_N, however, it was not applicable to 5 nm thick AlGa_N. A higher density of surface (and interface) states was found for 5 nm thick AlGa_N, leading to a thinner tunneling barrier. Direct tunneling might occur significantly for 5 nm thick AlGa_N while TD-related trap assisted tunneling was dominant for 10 nm thick AlGa_N. Reducing the density of acceptor-like defects and minimizing the incorporation of oxygen atoms in AlGa_N is highly required during the ALD growth. Even though the diode characteristics are not sufficiently good, the results obtained from this work will be meaningful for the understanding of the properties of ALD-AlGa_N, in terms of both devices and materials. For example, the ALD growth can be applied to nanostructured layers with uniform thickness. In such nanoscale devices, the information obtained from the ALD-AlGa_N layer is helpful in understanding device performance.

Author Contributions: Conceptualization, H.K.; methodology, H.K. and B.J.C.; investigation, H.K. and S.C.; writing—original draft, H.K.; writing—review and editing, H.K. and B.J.C. All authors have read and agreed to the published version of the manuscript.

Funding: This work was supported by the Basic Science Research Program through the National Research Foundation of Korea (NRF) funded by the Ministry of Education (2017R1D1A1B03030400).

Conflicts of Interest: The authors declare no conflict of interest.

References

1. Ibbetson, J.; Fini, P.; Ness, K.; DenBaars, S.; Speck, J.; Mishra, U. Polarization effects, surface states, and the source of electrons in AlGa_N/Ga_N heterostructure field effect transistors. *Appl. Phys. Lett.* **2000**, *77*, 250–252. [[CrossRef](#)]
2. Ambacher, O.; Smart, J.; Shealy, J.; Weimann, N.; Chu, K.; Murphy, M.; Schaffl, W.; Eastman, L.; Dimitrov, R.; Wittmer, L.; et al. Two-dimensional electron gases induced by spontaneous and piezoelectric polarization charges in N- and Ga-face AlGa_N/Ga_N heterostructures. *J. Appl. Phys.* **1999**, *85*, 3222–3233. [[CrossRef](#)]
3. Ambacher, O.; Majewski, J.; Miskys, C.; Link, A.; Hermann, M.; Eickhoff, M.; Stutzmann, M.; Bernardini, F.; Fiorentini, V.; Tilak, V.; et al. Pyroelectric properties of Al(In)Ga_N/Ga_N hetero- and quantum well structures. *J. Phys. Condens. Matter.* **2002**, *14*, 3399–3434. [[CrossRef](#)]
4. Marcon, D.; Viaene, J.; Favia, P.; Bender, H.; Kang, X.; Lenci, S.; Decoutere, S. Reliability of AlGa_N/Ga_N HEMTs: Permanent leakage current increase and output current drop. *Microelectron. Reliab.* **2012**, *52*, 2188–2193. [[CrossRef](#)]
5. Usami, S.; Ando, Y.; Tanaka, A.; Nagamatsu, K.; Deki, M.; Kushimoto, M.; Nitta, S.; Honda, Y.; Amano, H.; Sugawara, Y.; et al. Correlation between dislocations and leakage current of p-n diodes on a free-standing Ga_N substrate. *Appl. Phys. Lett.* **2018**, *112*, 182106. [[CrossRef](#)]
6. Simpkins, B.; Yu, E.; Waltereit, P.; Speck, J. Correlated scanning Kelvin probe and conductive atomic force microscopy studies of dislocations in gallium nitride. *J. Appl. Phys.* **2003**, *94*, 1448–1453. [[CrossRef](#)]
7. Besendörfer, S.; Meissner, E.; Lesnik, A.; Friedrich, J.; Dadgar, A.; Erlbacher, T. Methodology for the investigation of threading dislocations as a source of vertical leakage in AlGa_N/Ga_N-HEMT heterostructures for power devices. *J. Appl. Phys.* **2019**, *125*, 095704. [[CrossRef](#)]

8. Hashizume, T.; Kotani, J.; Hasegawa, H. Leakage mechanism in GaN and AlGa_N Schottky interfaces. *Appl. Phys. Lett.* **2004**, *84*, 4884–4886. [[CrossRef](#)]
9. Yan, D.; Lu, H.; Cao, D.; Chen, D.; Zhang, R.; Zheng, Y. On the reverse gate leakage current of AlGa_N/Ga_N high electron mobility transistors. *Appl. Phys. Lett.* **2010**, *97*, 153503. [[CrossRef](#)]
10. Ha, W.; Chhajed, S.; Oh, S.; Hwang, S.; Kim, J.; Lee, J.; Kim, K. Analysis of the reverse leakage current in AlGa_N/Ga_N Schottky barrier diodes treated with fluorine plasma. *Appl. Phys. Lett.* **2012**, *100*, 132104.
11. Ren, J.; Yan, D.; Zhai, Y.; Mou, W.; Gu, X. Comparison of electrical characteristics between AlGa_N/Ga_N and lattice-matched InAlN/Ga_N heterostructure Schottky barrier diodes. *Microelectron. Rel.* **2016**, *61*, 82–86. [[CrossRef](#)]
12. Huang, S.; Liu, X.; Wei, K.; Liu, G.; Wang, X.; Sun, B.; Yang, X.; Shen, B.; Liu, C.; Liu, S.; et al. O₃-sourced atomic layer deposition of high quality Al₂O₃ gate dielectric for normally-off Ga_N metal-insulator-semiconductor high electron-mobility transistors. *Appl. Phys. Lett.* **2015**, *106*, 033507. [[CrossRef](#)]
13. George, S. Atomic layer deposition: An overview. *Chem. Rev.* **2010**, *110*, 111–131. [[CrossRef](#)]
14. Ozgit, C.; Donmez, I.; Alevli, M.; Biyikli, N. Atomic layer deposition of Ga_N at low temperatures. *J. Vac. Sci. Technol. A* **2013**, *30*, 01A124. [[CrossRef](#)]
15. Ozgit-Akgun, C.; Goldenberg, E.; Okyay, A.; Biyikli, N. Hollow cathode plasma-assisted atomic layer deposition of crystalline AlN, Ga_N and Al_xGa_{1-x}N thin films at low temperatures. *J. Mater. Chem. C* **2014**, *2*, 2123–2236. [[CrossRef](#)]
16. Kim, H.; Kim, N.; An, S.; Yoon, H.; Choi, B. Improved interfacial properties of thermal atomic layer deposited AlN on Ga_N. *Vacuum* **2019**, *159*, 379–381. [[CrossRef](#)]
17. Tung, R. Recent advances in Schottky barrier concepts. *Mater. Sci. Eng. R.* **2001**, *35*, 1–138. [[CrossRef](#)]
18. Qiao, D.; Yu, L.; Lau, S.; Redwing, J.; Lin, J.; Jiang, H. Dependence of Ni/AlGa_N Schottky barrier height on Al mole fraction. *J. Appl. Phys.* **2000**, *87*, 801–804. [[CrossRef](#)]
19. Suzue, K.; Mohammad, S.; Fan, Z.; Kim, W.; Aktas, O.; Botchkarev, A.; Morkoç, H. Electrical conduction in platinum–gallium nitride Schottky diodes. *J. Appl. Phys.* **1996**, *80*, 4467–4478. [[CrossRef](#)]
20. Donoval, D.; Chvála, A.; Šramatý, R.; Kováč, J.; Morvan, E.; Dua, C.; DiForte-Poisson, M.; Kordoš, P. Transport properties and barrier height evaluation in Ni/InAlN/Ga_N Schottky diodes. *J. Appl. Phys.* **2011**, *109*, 063711. [[CrossRef](#)]
21. Pelá, R.; Caetano, C.; Marques, M.; Ferreira, L.; Furthmüller, J.; Teles, L. Accurate band gaps of AlGa_N, InGa_N, and AlInN alloys calculations based on LDA-1/2 approach. *Appl. Phys. Lett.* **2011**, *98*, 151907. [[CrossRef](#)]
22. Wagner, A.; Young, W.; Sugerman, A. A note on the correlation between the Schottky-diode barrier height and the ideality factor as determined from I-V measurements. *IEEE Electron Device Lett.* **1983**, *4*, 320–322. [[CrossRef](#)]
23. Belyaev, A.; Boltovets, N.; Ivanov, V.; Klad'ko, V.; Konakova, R.; Kudrik, Y.; Kuchuk, A.; Milenin, V.; Sveshnikov, Y.; Sheremet, V. Mechanism of dislocation-governed charge transport in Schottky diodes based on gallium nitride. *Semiconductors* **2008**, *42*, 689–693. [[CrossRef](#)]
24. Tarsa, E.; Heying, B.; Wu, X.; Fini, P.; DenBarrs, S.; Speck, J. Homoepitaxial growth of Ga_N under Ga-stable and N-stable conditions by plasma-assisted molecular beam epitaxy. *J. Appl. Phys.* **1997**, *82*, 5472–5479. [[CrossRef](#)]
25. Moseley, M.; Allerman, A.; Crawford, M.; Wierer, J., Jr.; Smith, M.; Biedermann, L. Electrical current leakage and open-core threading dislocations in AlGa_N-based deep ultraviolet light-emitting diodes. *J. Appl. Phys.* **2014**, *116*, 053104. [[CrossRef](#)]
26. Michaelson, H. The work function of the elements and its periodicity. *J. Appl. Phys.* **1977**, *48*, 4729–4733. [[CrossRef](#)]
27. Lee, C.; Lin, Y.; Liu, D. Schottky barrier height and surface state density of Ni/Au contacts to (NH₄)₂S_x-treated n-type Ga_N. *Appl. Phys. Lett.* **2001**, *79*, 2573–2575. [[CrossRef](#)]
28. Hasegawa, H.; Susumu, O. Mechanism of anomalous current transport in n-type Ga_N Schottky contacts. *J. Vac. Sci. Technol. B.* **2002**, *20*, 1647–1655. [[CrossRef](#)]
29. Gordon, L.; Miao, M.; Chowdhury, S.; Higashiwaki, M.; Mishra, U.; Walle, C. Distributed surface donor states and the two-dimensional electron gas at AlGa_N/Ga_N heterojunctions. *J. Phys. D Appl. Phys.* **2010**, *43*, 505501. [[CrossRef](#)]

30. Hashizume, Y.; Kotani, J.; Basile, A.; Kaneko, M. Surface control process of AlGa_N for suppression of gate leakage currents in AlGa_N/Ga_N heterostructure field effect transistors. *Jpn. J. Appl. Phys.* **2006**, *45*, L111–L113. [[CrossRef](#)]
31. Özdemir, A.; Türüt, A.; Kökce, A. The interface state energy distribution from capacitance–frequency characteristics of gold/n-type Gallium arsenide Schottky barrier diodes exposed to air. *Thin Solid Films* **2003**, *425*, 2010–2015. [[CrossRef](#)]
32. Lee, C.; Lin, C.; Lee, H.; Chen, P. Changes in surface state density due to chlorine treatment in Ga_N Schottky ultraviolet photodetectors. *J. Appl. Phys.* **2008**, *103*, 094504. [[CrossRef](#)]
33. Enisherlova, K.; Goryachev, V.; Rusak, T.; Kapilin, S. Study of the effect of passivation layers on capacitance of AlGa_N/Ga_N heterostructures. *Modern Electron. Mater.* **2016**, *2*, 131–137. [[CrossRef](#)]
34. He, Y.; Mi, M.; Zhang, M.; Wang, C.; Ma, X.; Hao, Y. Influence of Thermal Annealing on AlGa_N/Ga_N HEMT by Fluorine Plasma Treatment. In Proceedings of the 2016 13th China International Forum on Solid State Lighting: International Forum on Wide Bandgap Semiconductors China (SSLChina: IFWS), Beijing, China, 15–17 November 2016; IEEE: Piscataway, NJ, USA, 2016; pp. 116–119.
35. Miczek, M.; Mizue, C.; Hashizume, T.; Adamowicz, B. Effects of interface states and temperature on the C–V behavior of metal/insulator/AlGa_N/Ga_N heterostructure capacitors. *J. Appl. Phys.* **2008**, *103*, 104510. [[CrossRef](#)]
36. He, Y.; Wang, C.; Mi, M.; Zheng, X.; Zhang, M.; Zhao, M.; Zhang, H.; Chen, L.; Zhang, J.; Ma, Z.; et al. Recessed-gate quasi-enhancement-mode AlGa_N/Ga_N high electron mobility transistors with oxygen plasma treatment. *Chin. Phys. B.* **2016**, *25*, 117305. [[CrossRef](#)]
37. Zhang, K.; Chen, X.; Mi, M.; Zhao, S.; Chen, Y.; Zhang, J.; Ma, X.; Hao, Y. Enhancement-mode AlGa_N/Ga_N HEMTs with thin and high Al composition barrier layers using O₂ plasma implantation. *Phys. Status Solidi A.* **2015**, *212*, 1081–1085. [[CrossRef](#)]
38. Lv, Y.; Lin, Z.; Corrigan, T.; Zhao, J.; Cao, Z.; Meng, L.; Luan, C.; Wang, Z.; Chen, H. Extraction of AlGa_N/Ga_N heterostructure Schottky diode barrier heights from forward current-voltage characteristics. *J. Appl. Phys.* **2011**, *109*, 074512. [[CrossRef](#)]
39. Hung, T.; Krishnamoorthy, S.; Esposto, M.; Nath, D.; Park, P.; Rajan, S. Interface charge engineering at atomic layer deposited dielectric/III-nitride interfaces. *Appl. Phys. Lett.* **2013**, *102*, 072105. [[CrossRef](#)]



© 2020 by the authors. Licensee MDPI, Basel, Switzerland. This article is an open access article distributed under the terms and conditions of the Creative Commons Attribution (CC BY) license (<http://creativecommons.org/licenses/by/4.0/>).